Optical fiber Fabry-Perot interferometer cavity fabricated by femtosecond laser micromachining and fusion splicing for refractive index sensing

C. R. Liao, T.Y. Hu, and D. N. Wang*

The Hong Kong Polytechnic University, Hung Hom, Kowloon, Hong Kong, China
*eednwang@polyu.edu.hk

Abstract: We demonstrate a fiber in-line Fabry-Perot interferometer cavity sensor for refractive index measurement. The interferometer cavity is formed by drilling a micro-hole at the cleaved fiber end facet, followed by fusion splicing. A micro-channel is inscribed by femtosecond laser micromachining to vertically cross the cavity to allow liquid to flow in. The refractive index sensitivity obtained is ~994 nm/RIU (refractive index unit). Such a device is simple in configuration, easy for fabrication and reliable in operation due to extremely low temperature cross sensitivity of ~4.8×10^{-6} RIU/°C.

OCIS codes: (320.7090) Ultrafast laser; (060.2370) Fiber optics sensors; (120.0120) Instrumentation, measurement, and metrology.

References and links

1. Z. X. Gao, A. Adnet, Z. Zhang, F. G. Sun, and C. P. Grover, "Monitoring changes in the refractive index of gases by means of a fiber optic Fabry-Perot interferometer sensor," Sensors Actuat. A-Phys. **118**, 117–182 (2005).
2. P. Domachuk, I. C. M. Littler, M. Cronin-Golomb, and B. J. Eggleton, "Compact resonant integrated microfluidic refractometer," Appl. Phys. Lett. **88**(9), 093513 (2006).
3. T. Wei, Y. Han, Y. Li, H. L. Tsai, and H. Xiao, "Temperature-insensitive miniaturized fiber inline Fabry-Perot interferometer for highly sensitive refractive index measurement," Opt. Express **16**(8), 5764–5769 (2008).
4. J. Villatoro, V. Finazzi, G. Coviello, and V. Pruneri, "Photonic-crystal-fiber-enabled micro-Fabry-Perot interferometer," Opt. Lett. **34**(16), 2441–2443 (2009).
5. J. Ma, J. Ju, L. Jin, W. Jin, and D. Wang, "Fiber-tip micro-cavity for temperature and transverse load sensing," Opt. Express **19**(13), 12418–12426 (2011).
6. M. S. Ferreira, L. Coelho, K. Schuster, J. Kobelke, J. L. Santos, and O. Frazão, "Fabry-Perot cavity based on a diaphragm-free hollow-core silica tube," Opt. Lett. **36**(20), 4029–4031 (2011).
7. Z. Ran, Y. J. Rao, J. Zhang, Z. Liu, and B. Xu, "A miniature fiber-optic refractive-index sensor based on laser-machined Fabry-Perot interfermmeter tip," J. Lightwave Technol. **27**(23), 5426–5429 (2009).
8. H. Y. Choi, G. Mudhana, K. S. Park, U.-C. Paek, and B. H. Lee, "Cross-talk free and ultra-compact fiber optic sensor for simultaneous measurement of temperature and refractive index," Opt. Express **18**(1), 141–149 (2010).
9. K. Mileńko, D. J. Hu, P. P. Shum, T. Zhang, J. L. Lim, Y. Wang, T. R. Woliński, H. Wei, and W. Tong, "Photonic crystal fiber tip interferometer for refractive index sensing," Opt. Lett. **37**(8), 1373–1375 (2012).
10. Z. L. Ran, Y. J. Rao, W. J. Liu, X. Liao, and K. S. Chiang, "Laser-micromachined Fabry-Perot optical fiber tip sensor for high-resolution temperature-independent measurement of refractive index," Opt. Express **16**(3), 2252–2263 (2008).
11. K. M. Davis, K. Miura, N. Sugimoto, and K. Hirao, "Writing waveguides in glass with a femtosecond laser," Opt. Lett. **21**(21), 1729–1731 (1996).
12. W. J. Chen, S. M. Eaton, H. Zhang, and P. R. Herman, "Broadband directional couplers fabricated in bulk glass with high repetition rate femtosecond laser pulses," Opt. Express **16**(15), 11470–11480 (2008).
13. Y. Kondo, K. Nouchi, T. Mitsuyu, M. Watanabe, P. G. Kazansky, and K. Hirao, "Fabrication of long-period fiber gratings by focus irradiation of infrared femtosecond laser pulses," Opt. Lett. **24**(10), 646–648 (1999).
14. S. J. Mihailov, C. W. Smelser, P. Lu, R. B. Walker, D. Grobnic, H. Ding, G. Henderson, and J. Unruh, "Fiber Bragg gratings made with a phase mask and 800-nm femtosecond radiation," Opt. Lett. **28**(12), 995–997 (2003).
15. S. J. Liu, L. Jin, W. Jin, D. N. Wang, C. R. Liao, and Y. Wang, "Structural long period gratings made by drilling micro-holes in photonic crystal fibers with a femtosecond infrared laser," Opt. Express **18**(6), 5496–5503 (2010).
16. M. Park, S. Lee, W. Ha, D. K. Kim, W. Shin, I. B. Sohn, and K. Oh, "Ultracompact intrinsic micro air-cavity fiber Mach-Zehnder Interferometer," IEEE Photon. Technol. Lett. **21**(15), 1027–1029 (2009).

#172051 - $15.00 USD Received 6 Jul 2012; revised 6 Sep 2012; accepted 11 Sep 2012; published 20 Sep 2012

17. Y. Wang, M. W. Yang, D. N. Wang, S. J. Liu, and P. X. Lu, "Fiber in-line Mach-Zehnder interferometer fabricated by femtosecond laser micromachining for refractive index measurement with high sensitivity," J. Opt. Soc. Am. B **27**(3), 370–374 (2010).
18. J. Yang, L. Jiang, S. Wang, Q. Chen, B. Li, and H. Xiao, "Highly sensitive refractive index optical fiber sensors fabricated by a femtosecond laser," IEEE Photonics J. **3**(6), 1189–1197 (2011).
19. H. Y. Fu, K. M. Zhou, P. Saffari, C. B. Mou, L. Zhang, S. L. He, and I. Bennion, "Microchanneled chirped fiber Bragg grating formed by femtosecond laser aided chemical etching for refractive index and temperature measurements," IEEE Photon. Technol. Lett. **20**(19), 1609–1611 (2008).
20. X. Fang, C. R. Liao, and D. N. Wang, "Femtosecond laser fabricated fiber Bragg grating in microfiber for refractive index sensing," Opt. Lett. **35**(7), 1007–1009 (2010).
21. V. Bhatia and A. M. Vengsarkar, "Optical fiber long-period grating sensors," Opt. Lett. **21**(9), 692–694 (1996).
22. J. F. Ding, A. P. Zhang, L. Y. Shao, J. H. Yan, and S. L. He, "Fiber-taper seeded long-period grating pair as a highly sensitive refractive index sensor," IEEE Photon. Technol. Lett. **17**(6), 1247–1249 (2005).
23. R. Jha, J. Villatoro, G. Badenes, and V. Pruneri, "Refractometry based on a photonic crystal fiber interferometer," Opt. Lett. **34**(5), 617–619 (2009).
24. Z. B. Tian, S. S. H. Yam, and H. P. Loock, "Refractive index sensor based on an abrupt taper Michelson interferometer in a single-mode fiber," Opt. Lett. **33**(10), 1105–1107 (2008).

1. Introduction

Optical fiber Fabry-Perot interferometer (FPI) cavity has been attractive for many sensor applications owing to its miniature size, in-line structure, linear response, high sensitivity and convenient reflection mode of detection [1–10]. To enable effective refractive index (RI) sensing, the optical fiber FPI should be constructed into a tip device for flexible liquid immersion or built with an open micro-cavity to allow liquid to flow in. In such schemes, the conventional single mode fiber (SMF) needs to be incorporated with in-fiber mirrors [7], or spliced with a section of photonic crystal fiber [8, 9]. However, these fabrication methods are rather complicated or with relatively high cost. In recent years, near-IR femtosecond (fs) laser has been widely used for fabricating photonic devices in transparent materials such as bulk glasses [11, 12] and different types of optical fibers [13–15]. Many micro-cavities have been fabricated in optical fiber by using fs laser micromachining and operated as fiber in-line interferometers, such as FPIs [3, 7, 10] and Mach-Zehnder interferometers (MZIs) [16–18]. However, such fiber in-line interferometers, directly fabricated by fs laser ablation, usually exhibit rather rough cavity surface and poor mechanical strength.

In this paper, a fiber in-line FPI cavity fabricated by using fs laser micromachining together with fusion splicing is presented for refractive index (RI) sensing. The FPI cavity is formed by drilling a micro-hole at the end facet of SMF, followed by fusion splicing, and finally inscribing a micro-channel by fs laser micromachining to vertically cross the cavity and allow the RI liquid to flow in. Such a RI sensor is simple in structure, easy for fabrication and reliable in operation. The RI sensitivity obtained is ~994nm/RIU with extremely low temperature cross-sensitivity of ~4.8×10^{-6} RIU/°C.

2. Operation principle of the system

Figure 1 shows the schematic diagram of the FPI sensor system proposed, in which a hollow sphere with vertical opening serves as the FP cavity. The incident light beam along the SMF is reflected by the two surfaces of the sphere respectively and recombined in the fiber core, resulting in an interference pattern at the output.

#172051 - $15.00 USD Received 6 Jul 2012; revised 6 Sep 2012; accepted 11 Sep 2012; published 20 Sep 2012

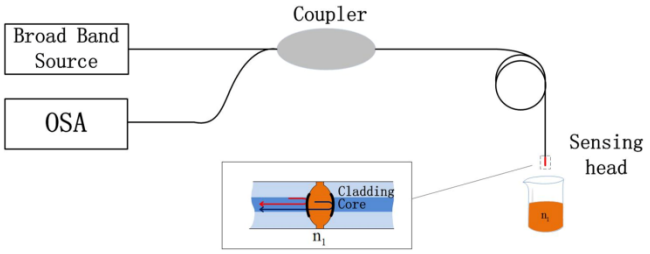

Fig. 1. Experimental setup for RI measurement. The inset shows the schematic diagram of the fiber FPI.

Assuming that the light intensities of the reflected beams by the two surfaces of the FP cavity are I_1 and I_2, respectively, the interference signal intensity is:

$$I = I_1 + I_2 + 2\sqrt{I_1 I_2}\cos(\frac{4\pi nL}{\lambda} + \varphi_0) \quad (1)$$

where λ is the wavelength of the incident light, n is the RI of the cavity medium, L is cavity length and φ_0 is the initial phase of the interference. At the fringe dip positions, the phase difference of the two reflected light beams satisfies the condition,

$$\frac{4\pi nL}{\lambda_m} + \varphi_0 = (2m+1)\pi \quad (2)$$

where m is an integer, λ_m is the wavelength of the m^{th} order interference dip. The fringe spacing in the spectrum can then be expressed as,

$$\Lambda = \frac{\lambda^2}{2nL} \quad (3)$$

3. Device fabrication

In the device fabrication, fs laser pulses (λ = 800 nm) of 120 fs at the repetition rate of 1 kHz were focused onto the fiber end facet by a 20 × objective lens with NA value of 0.5 and working distance of 2.1mm. The pulse energy used in the experiment was ~2 μJ. A CCD camera was employed to monitor the fabrication process and record the sample morphology. A section of standard SMF-28 with the core diameter of 8.2 μm and the nominal effective RI of 1.4682 (at 1550 nm) was mounted on a computer controlled three-dimensional translation stage with a 40-nm resolution. The following steps were adopted in the fabrication process as illustrated in Fig. 2. Firstly, fs laser drilled a micro-hole of ~1 μm in diameter at the center of the cleaved fiber end facet, and the fiber tip obtained was then spliced together with another cleaved SMF tip without micro-hole by a fusion splicer (ERICSSON FSU975), with fusing current and fusing duration of 16.3 mA and 2.0 s respectively. The hollow sphere formed had a diameter of ~60 μm. Finally, a micro-channel of ~38 μm in diameter was machined to vertically cross the FP cavity, which allowed the RI liquid to readily flow in or out of the cavity. In the micro-channel fabrication process, laser beam was firstly focused on the top fiber surface at the micro-cavity position, scanned at a speed of 2 μm/s with a scanning distance of 40 μm, in parallel to the fiber core axis. After one scanning cycle, the laser beam was shifted by 10 μm, in perpendicular to the fiber axis until a 40μm × 40μm square area was drilled through, to create the top part of the micro-channel. The fiber was then rotated by 180° to allow fabrication of the bottom part of the micro-cavity, following the same procedure as mentioned above.

#172051 - $15.00 USD Received 6 Jul 2012; revised 6 Sep 2012; accepted 11 Sep 2012; published 20 Sep 2012

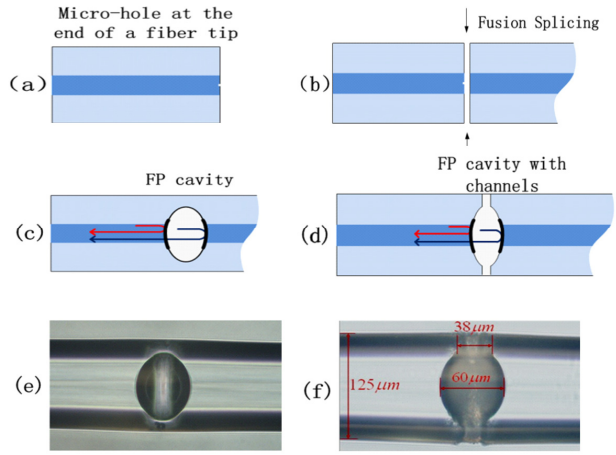

Fig. 2. Fiber in line FPI cavity fabrication process. (a) The fs laser creates a micro-hole of ~1 μm in diameter at the center of cleaved fiber end facet. (b) The fiber tip with the micro-hole spliced together with another cleaved SMF tip. (c) FP cavity formed. (d) To fabricate a micro-channels to vertically cross the micro-cavity. (e) Microscope image of the fiber in-line FPI cavity without the micro-channel. (f) Microscope image of the fiber in-line FPI cavity with the micro-channel.

4. Experimental results and discussion

The RI measurement by the use of fiber in-line FP cavity was carried out at room temperature by immersing the sensor head in the RI liquids. Each time after the measurement, the device was rinsed with Propyl alcohol carefully until the original spectrum was restored and no residual liquid was left. The reflection spectra were monitored in real-time with an optical spectrum analyzer (OSA) with a resolution of 0.01 nm. Figure 3(a) shows the reflection spectra corresponding to the RI values of 1.315, 1.32 and 1.325, respectively, and a red shift of dip wavelength can be clearly observed. The transmission dip wavelength corresponding to different RI values within the range between 1.31 and 1.39 are demonstrated in Fig. 3(b), where a good linear relationship with the linearity of 99.9% is obtained. The RI sensitivity obtained is ~994 nm/RIU, which is comparable to that of FPIs reported by other groups [1–3, 7], superior to that of the fiber RI sensors based on fiber Bragg gratings [19, 20], long-period fiber gratings [21] and conventional fiber interferometers [22–24], and much lower than that of the fiber open-cavity MZI, which reaches ~9370 nm/RIU [17]. This is due to the fact that for FPI, the sensitivity is inversely proportional to the RI value of the cavity medium, whereas for MZI, it is inversely proportional to the RI difference of the cavity medium and the fiber core, which is much smaller than the RI of the cavity medium itself.

The temperature influence on the FPI cavity RI sensor has been investigated by placing the fiber tip in an electrical oven and gradually increasing the temperature from 24 to 100 °C. The temperature sensitivity obtained is ~4.8 pm/°C near the wavelength position of 1554 nm, as shown in Fig. 4. Based on the RI sensitivity of ~994 nm/RIU, the temperature cross-sensitivity of the sensor is ~4.8×10^{-6} RIU/°C. The temperature sensitivity of the fiber FPI sensor can be deduced from Eq. (2) as

$$\frac{d\lambda_m}{dT} = \frac{4}{2m+1}\left(\frac{dn}{dT}L + \frac{dL}{dT}n\right) \tag{4}$$

where *dn/dt* is the thermo-optic coefficient of cavity medium and *dL/dT* is the thermal-expansion coefficient of fiber material, ~0.55×10^{-6}/°C for SMF-28 fiber. If the cavity medium is air, the thermo-optic coefficient of air is tiny and thus the term *(dn/dT)L* in the

#172051 - $15.00 USD Received 6 Jul 2012; revised 6 Sep 2012; accepted 11 Sep 2012; published 20 Sep 2012

above equation is negligible. Thermal-expansion effect plays a leading role in the temperature sensitivity.

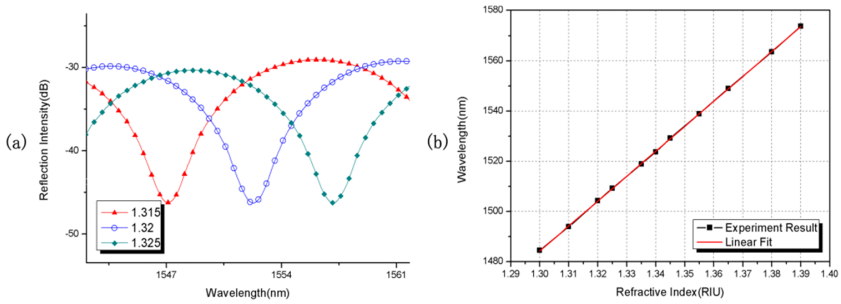

Fig. 3. (a) The reflection spectrum at RI = 1.315, 1.32 and 1.325, respectively (b) RI response of the sensor.

(b) RI response of the sensor.

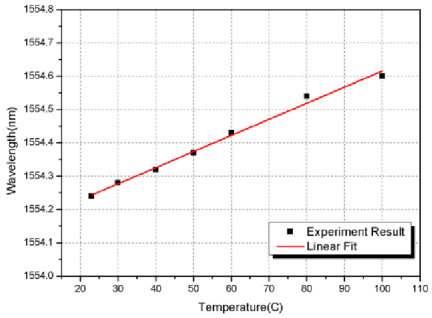

Fig. 4. Temperature response of the sensor

By changing the size of initial micro-hole and the fusion splicing parameters, the hollow sphere of different sizes and hence different cavity lengths can be created. Figure 5(a) shows three hollow spheres with different cavity lengths of 30, 65 and 93 μm respectively, corresponding to the initial micro-hole diameter of 1, 1 and 10 μm, the fusion current of 15.3, 16.8 and 17.3 mA, and the fusion duration of 1.5, 2.0, and 2.0 s respectively. The reflection spectra corresponding to different cavity lengths are displayed in Fig. 5(b). It can be found from this figure that, with the increase of cavity length from 30 μm to 93 μm, the fringe spacing around 1550 nm is decreased from 39.3 nm to 12.9 nm. The fringe spacing variation around 1550 nm with the air-cavity length was calculated according to Eq. (3), and the results obtained are shown in Fig. 5(c), where the black line stands for the calculated results and the red squares represent the experimental values obtained in Fig. 5(b). The experimental results agree well with the simulations based on FPI theory.

Figure 5(b) shows that the reflection intensity monotonically goes up with the increase of cavity length. This is due to the fact that with a larger radius of the hollow sphere, the two reflection surfaces within the fiber core are nearly in parallel and hence the reflected light intensity can be enhanced. However, the fringe visibility does not change in a monotonic manner when the cavity length is increased as it depends also on surface reflectivity and propagation loss in the cavity.

The size of the vertical micro-channel should be properly chosen to facilitate the RI liquid flow in and out of the FPI cavity. The micro-channel size of 20 and 38 μm were tested in the experiment, and the time taken for the liquid to be fully filled in the cavity was 15 minutes and a few seconds, respectively. The dependence of the filling time of the liquid on the size of micro-channel is due to the dependence of air pressure inside the micro-cavity on the size of

#172051 - $15.00 USD Received 6 Jul 2012; revised 6 Sep 2012; accepted 11 Sep 2012; published 20 Sep 2012

micro-channel. When the sample is immersed into the liquid, the air pressure inside the micro-cavity would prevent the liquid to flow in. If the micro-channel size is small, the air would slowly escape from the cavity and thus the filling time of the liquid is long. When the channel size becomes large, the air can quickly escape from the micro-cavity and a short filling time of the liquid can be achieved. Since the micro-channel is located purely in the cladding area, its size has no essential effects on the interference spectrum. However, a large channel size would reduce the robustness of the device.

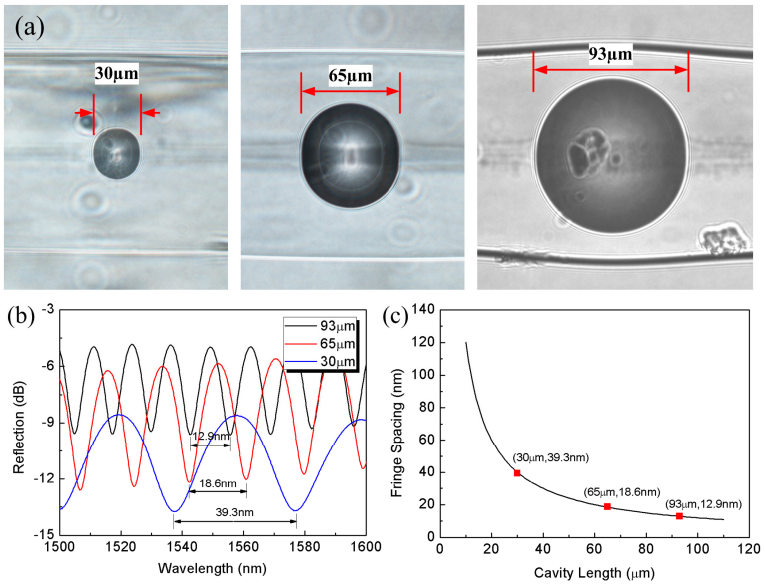

Fig. 5. (a) Microscope images of the FPI cavity with length of 30, 65 and 93 μm, respectively. (b) Reflection spectra of fiber in-line FPI with different cavity lengths. (c) Simulated fringe spacing as a function of cavity length at the wavelength of 1550 nm. The black line is the calculation result and the red square shows the experimentally obtained value.

It should be mentioned that the system actually has two FP cavities. The second FP cavity is formed by the hollow sphere surface and the fiber end immersed in the liquid. Since the reflected light beam from the hollow sphere surface is divergent, and a large curvature of the hollow sphere surface corresponds to a large reflection light divergence, the interference fringe pattern of the second FP cavity is critically dependent on the cavity length. When the cavity length is large, the reflected light beam intensity is very small, which leads to an extremely poor fringe visibility and as a result, the corresponding fringe pattern can hardly be observed. In our experiment, the second cavity length is ~40 mm and the fiber end immersed in the liquid is not cleaved, thus no corresponding fringe can be observed.

5. Conclusion

In conclusion, a fiber in-line FPI cavity sensor has been proposed and demonstrated for RI measurement. The change of liquid RI value causes the change of the optical path difference of FPI, which in turn leads to an interference spectrum shift. The RI sensitivity achieved in the experiment is ~994 nm/RIU, and the temperature cross-sensitivity is ~4.8×10^{-6} RIU/°C. Such a device is simple in structure, easy in fabrication and reliable in operation.

Acknowledgment

This work was supported by the Hong Kong SAR government through a GRF (general research fund) grant PolyU 5298/10E and The Hong Kong Polytechnic University research grant 4-ZZE3. The authors also like to thank Dr. Ying Wang for helpful discussions.

#172051 - $15.00 USD Received 6 Jul 2012; revised 6 Sep 2012; accepted 11 Sep 2012; published 20 Sep 2012